AIAA Journal

VOLUME 2 SEPTEMBER 1964 NUMBER 9

A Transonic Experiment at Hypersonic Speed

S. C. TRAUGOTT*
The Martin Company, Baltimore, Md.

Cylindrically blunted wedges were tested in a hotshot tunnel at various angles of attack at a Mach number of about twenty. The geometry was so arranged that the sonic point occurred either on the nose or much further downstream on the corner terminating the body, depending on angle of attack. Both surface pressures and shock shapes were obtained over the range in incidence associated with this large change in sonic point body thickness. The rearward shift of the sonic point was found to have very little effect on the flow for a relatively slender blunted wedge. The role of asymmetry in the stagnation region was explored by comparing a nonslender blunted wedge at small incidence to the slender wedge at large incidence. Coordinates are discussed which allow representation of both shock shapes and surface pressures of small afterbody flow deflection theory together with blast wave theory. In these coordinates, pressure and shock from the present large flow deflection experiments on the slender wedge (up to loss of asymptotic wedge flow) also correlate, independent of the position of the sonic point.

Nomenclature

C_D = nose drag coefficient
d = nose thickness or diameter
M_∞ = flight Mach number
p = surface pressure
p_{max} = stagnation pressure behind a perpendicular shock
p_{asy} = asymptotic surface pressure far downstream
R = nose radius
S = distance along the body measured from the stagnation point
T = temperature
T_∞ = temperature ahead of the shock
x = distance along the direction of flow measured from the stagnation point
y = distance, perpendicular to the flow direction, from stagnation streamline to shock
α = angle of attack, measured from flow direction to afterbody plane of symmetry
γ = ratio of specific heats
Δ = shock standoff distance
δ = afterbody flow deflection angle
ρ = density
ρ_0 = reference density, $\rho_0 = 1.2505 \times 10^{-3}$ g/cm^3
ρ_∞ = density ahead of the shock
ϕ = body surface angle measured from the normal to the flow direction
θ = asymptotic shock angle
ν = geometrical factor, equals 1 and 2 for two-dimensional and axisymmetric flow, respectively

I. Introduction

IT is well known that the flow field of a blunt body in hypersonic flight contains a transonic domain. Somewhere downstream of the stagnation region there will be a sonic line between shock and body. The location of the sonic point can be a useful guide for assessing surface pressures, and it can be used in a simple way to relate shock and body geometry.[1] The shape of the sonic line determines what, if any, influence the downstream, supersonic portions of the body exert on the upstream, subsonic nose flow.

Unfortunately, the transonic regime falls outside the regions for which relatively simple theoretical models are available. Further upstream, constant density theory prevails. Further downstream, hypersonic slender body theory becomes useful. The author is aware of only one method[2] that can give transonic information for blunt bodies to those without access to either automatic computing machines or experimental facilities. This method is inverse and fails for precisely that case where the location of the body sonic point is supposed to be easy, the case where the body has a corner. For such a body, even digital methods have only been applied to cases where the sonic point is known to be at the corner.[3, 4] Often we know that it is not there. Further, it is easy to invent bodies with two corners.

At present there is increasing interest in hypersonic lifting bodies. For a blunt body with transonic flow somewhere on the nose at zero incidence, there clearly will be some angle of attack for which the sonic point on the windward side has been forced to the downstream corner. Only involved numerical computations or experiment could predict this angle and what effect a large rearward migration of the sonic point would have on body pressures and shock shape. This obviously has an important bearing on the stability characteristics of the body. In attempting to assess such an effect, two experimental investigations are relevant.

Johnson[5] obtained shock shapes for a family of spherically blunted cones of various cone angles at zero incidence in hypersonic helium. For this symmetrical flow, it was found that there exists a critical cone angle below which the shock standoff distance is unaffected by increasing cone angle and above which shock standoff distance rapidly increases with

Received October 21, 1963; revision received April 24, 1964. The author gratefully acknowledges the cooperation and advice of S. M. Gottlieb and R. Phinney.

* Senior Scientist, Research Department. Member AIAA.

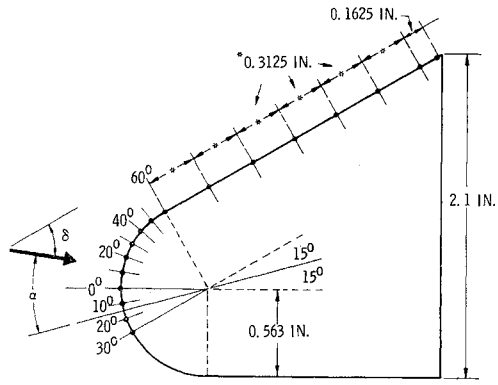

Fig. 1 Slender blunted wedge.

increasing cone angle. These results are interpreted in Ref. 5 in terms of a rather sudden rearward migration of the sonic point from the nose to the corner terminating the afterbody. No pressures were reported.

Zakkay and Fields[6] emphasized the importance of a movement of the sonic point out of the nose region in changing surface pressure. Their results for a cylinder-wedge at various angles of attack in air at $M_\infty = 6$ show clearly that the pressure distribution with the sonic point on the nose can be quite different from that obtained with the sonic point on the nearest downstream corner. Unfortunately, no data are reported in Ref. 6 within the range of incidence associated with the sonic point shift, nor is any information given about the associated shock geometry.

The present paper concerns an experiment designed to study the significance of a large change in position of the sonic point on the windward side of a hypersonic blunt body, induced by changes in angle of attack. Both surface pressures and schlieren photographs were obtained for a 15° semiangle cylinder wedge through the range in incidence associated with a sonic point shift of about 4 nose radii. Shock shapes were also obtained for a much blunter cylinder wedge in order to study the influence of asymmetry in the stagnation region. The two-dimensional body was chosen both to eliminate cross-flow complications for this asymmetric flow and to maximize the influence of the sonic point shift through the thicker entropy layer that exists on a two-dimensional configuration. Further, the pressure on hypersonic blunted wedges seems to have been somewhat neglected relative to that for blunted cones, though of no less importance.

II. Description of Experiment

The experiments were performed in the Martin hypervelocity tunnel. This is a capacitance-driven, 0.8-Mjoule hotshot tunnel. This facility has a 10° included angle conical nozzle with a 24-in.-diam test section. The useful gas core for the present conditions is estimated to have a diameter of about 10 in. The test gas was nitrogen. This was chosen to minimize complications due to dissociation, especially as far as shock shapes are concerned. Stagnation temperatures varied for the runs from 2900° to 2500°K, stagnation pressure ahead of the shock from 4300 to 3700 psia. The nominal test section Mach number was 20. The gas state ahead of the shock, averaged over all runs, corresponded to flight at $M_\infty = 19.5$ through nitrogen at $T_\infty = 42°$K and density $\rho_\infty/\rho_0 = 2.4 \times 10^{-4}$, as determined by the nitrogen Mollier chart in Ref. 7. Behind the shock there are real gas effects due to vibrational excitation, but the gas state is just short of dissociation (see Ref. 8). The average Reynolds number per inch ahead of the model shock was about 10,000, that at the model sonic point about 700. Useful flow time in the facility varied from about 15 to 20 msec.

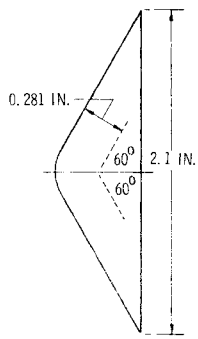

Fig. 2 Nonslender blunted wedge.

The pressure model was the 15° semiangle cylindrically blunted wedge shown in Fig. 1. It had a ratio of afterbody length to nose radius of 3.74 and a span of 6 in. Eighteen pressure taps were installed as indicated. These were arranged in three rows, one in the center of the span and the other two $\frac{5}{16}$ in. outboard. The wedge taps are located on the windward side of the afterbody at angle of attack. The furtherest downstream location was $\frac{1}{16}$ in. upstream of the corner, with two taps there in the outer rows. Variable reluctance diaphragm pressure transducers with a time constant of 1 msec were mounted inside the model; their amplified output signal was recorded on light sensitive oscillograph paper.

For comparison of shock shapes at the larger angles of attack with and without a large asymmetry in the stagnation region, another cylindrically blunted wedge was used, much less slender, with a semiangle of 60°. It is illustrated in Fig. 2. This body has the same ratio of distance between junction and corner to nose radius as the slender wedge, as well as the same span. Its nose radius is smaller as dictated by tunnel blockage considerations. It was not instrumented for pressure.

Optical information came from a double pass schlieren system† with a 10-ft-focal length and a 15-in.-diam mirror. Pictures of the shock were obtained with a xenon flash lamp flashing for approximately 1 μsec at 2-msec intervals. Quarter-inch images were obtained on 35-mm XXX film.

Pressure data were obtained on the slender wedge at angles of attack of $\alpha = 15°, 20°, 22°, 25°, 27°, 30°$, and 35°, which correspond to afterbody flow deflection angles on the windward side of $\delta = 30°, 35°, 37°, 40°, 42°, 45°$, and 50°. For reference, note that, with a perfect gas with $\gamma = 1.4$, a blunted wedge at $M_\infty = 20$ becomes asymptotically sonic on the surface for $\delta = 38.4°$, and the limit of wedge flow is reached for $\delta = 45.3°$. Schlieren photographs of the shock were obtained at $\alpha = 15°, 30°, 35°, 40°, 45°$, and 55° for the 15° wedge and at $\alpha = 0°$ and 10° for the 60° wedge.

The smallest ratio of span to body thickness occurs for the pressure model. This ratio varies with angle of attack from just over two at $\alpha = 55°$ to just under three at $\alpha = 15°$. Several runs with and without end-plates on the pressure model disclosed no optical or pressure evidence for any influence of the finite span.

III. Surface Pressures

The basic pressure results from this experiment are given by the open points in Fig. 3. All pressures p have been made dimensionless with stagnation pressure behind a perpendicular shock. They are given as functions of distance S along the body measured from the stagnation point, nondimensionalized by nose radius R, with afterbody flow deflection angle on the windward side δ as parameter. It was found that, over this range in δ, the stagnation point essentially rotated with the velocity vector, so that $S = 0$ may be identified with the point of tangency of the normal to the flow direction and the surface. The sonic pressure ratio for the

† Designed by R. Phinney.

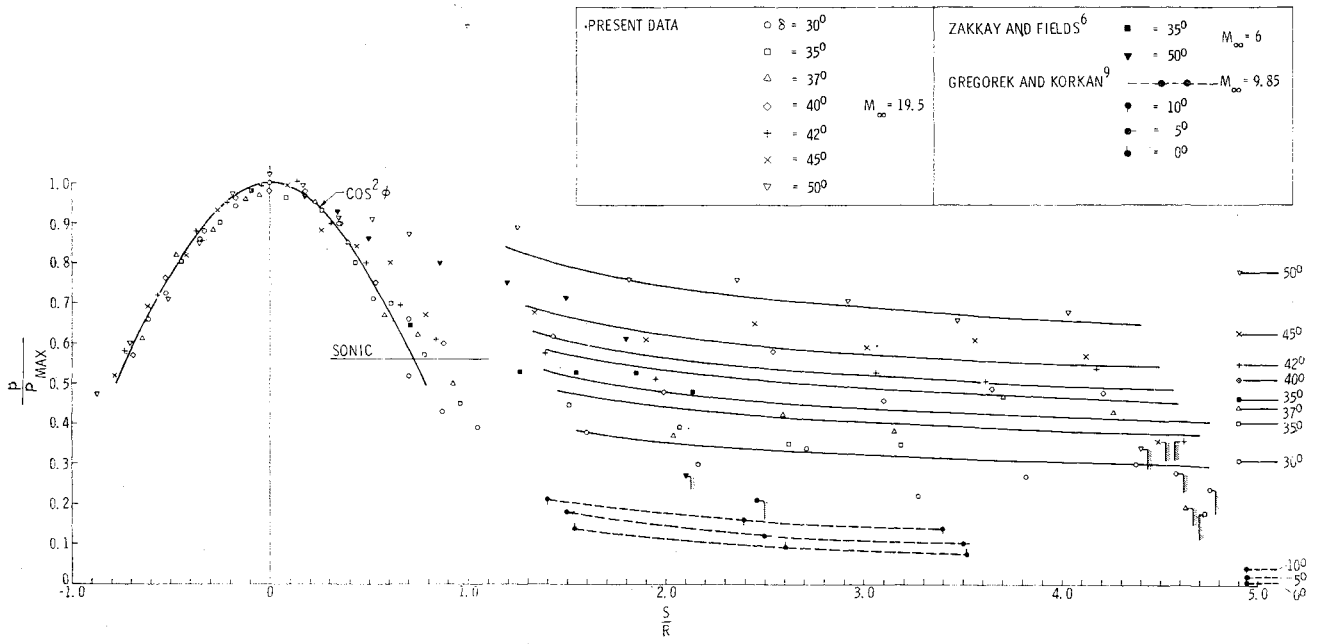

Fig. 3 Surface pressures.

present experiments has been indicated at $p/p_{max} = 0.56$, and calculated values of the asymptotic wedge pressures are also shown for each δ.‡ Each point in Fig. 3 represents an average at a particular location with the body at a particular angle of attack, with the average formed from all data for that location and angle.

Over the forebody, shadowside pressures as well as the windward pressures for small δ agree quite well with the modified Newtonian distribution $p/p_{max} = \cos^2\phi$. It is considered pointless to argue here whether this should or should not be so; we remark only that similar agreement is reported by Zakkay and Fields[6] at $M_\infty = 6$, that the results of Gregorek and Korkan[9] at $M_\infty = 9.85$ show measured pressures on a cylindrical nose considerably above modified Newtonian, that numerical solutions for a cylinder at $M_\infty = \infty$ by both Hamaker[10] and Fuller[11] show good agreement with it, and that data by Penland[12] are somewhat higher. From $\delta = 37°$ and higher, there is an increasing afterbody influence on windward nose pressures, at $\delta = 50°$ the Newtonian distribution is entirely irrelevant on that side, as pointed out in Ref. 6.

On the afterbody, the flagged points represent the output of the taps just ahead of the corner. The solid lines drawn through the afterbody data are determined from a correlation to be described. The lower points and dashed lines are taken from Fig. 3 of Gregorek and Korkan[9] for a cylindrically blunted plate at incidence with $\delta = 0°$, 5°, and 10°. The solid points come from Ref. 6 for $\delta = 35°$ and $\delta = 50°$, also with the corner pressure flagged. It is apparent that the present afterbody pressures follow the same trend with incidence regardless of the sonic point shift to the downstream corner, which has just begun at $\delta = 37°$ and is nearly complete for $\delta = 45°$. Even for $\delta = 50°$, the afterbody pressure, which is completely subsonic, appears to belong to the same family as those from Ref. 9, with very small flow deflection angles.

This is not true for the low Mach number data of Zakkay and Fields.[6] Their $\delta = 35°$ results are considerably above ours, but this is not unexpected if one considers the difference in the quantity $M_\infty \sin\theta$ between the experiments, with θ the asymptotic shock angle. This quantity is 4.3 for Ref. 6 and 13.1 for us, so that there should be a Mach number effect.

More significant is the difference apparent for $\delta = 50°$. With the surface subsonic, the location of the corner becomes a significant factor. It would seem that the subsonic pressures in Ref. 6 are determined primarily by the corner location. This is an important element to consider before attempting to extend the present results to other bodies.

It is interesting to note that the present data indicate pressures that are lower than the calculated asymptotic values. This overexpansion with respect to the asymptotic pressure becomes more pronounced with increasing δ and is not observed for the very small values of δ from Ref. 9. Similar behavior is known to occur for blunted cones. The observed overexpansion initially caused some alarm, since it was felt that overexpansion was restricted to axially symmetric bodies, and suspicions arose that the conical tunnel nozzle was responsible. An estimated conical flow correction, however, resulted in at most a 10% increase in the furtherest downstream pressure at the lowest angle of attack, with decreasing corrections for increasing δ. This correction was not applied to the data because of the uncertainties of the nozzle boundary layer. It would not, in any case, eliminate the overexpansion. Theoretical evidence that two-dimensional overexpansion is possible can be inferred from Hamaker's[10] computations for a cylinder perpendicular to the flow. In Fig. 1 of Ref. 10 one may locate on the cylinder the limiting characteristic given there with respect to the tangent point of an asymptotically sonic wedge. The limiting characteristic turns out to be 6° upstream of this tangent point, and thus, for this example, an asymptotically subsonic wedge can be found as an afterbody that is preceded by supersonic flow. This implies afterbody recompression, just as in the axially symmetric case.

IV. Shock Shapes

Superimposed shocks obtained from schlieren photographs at various angles of attack for both models are given in Fig. 4.

‡ The location of the stagnation point was determined by fitting for each angle of attack α the forebody pressures on the shadowside with a $\cos^2(S'/R + \text{const})$ distribution, with S' measured from the $\alpha = 0$ stagnation point. For each α, the constant turned out to be α within ±1°. Sonic pressure was determined from an isentropic expansion to $M = 1$ in the nitrogen Mollier chart of Ref. 7. The asymptotic pressure came from a real gas oblique shock calculation that gave shock angle and pressure behind the shock as a function of flow deflection angle. The resulting shock angles differed considerably from those for a perfect gas with $\gamma = 1.4$.

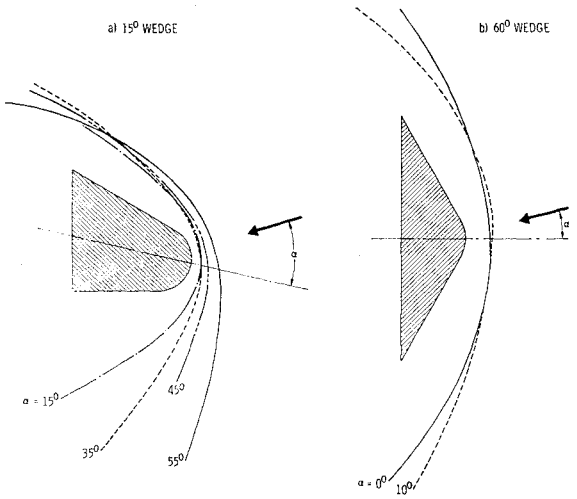

Fig. 4 Superposed shock shapes.

As just discussed, the sonic point shift to the downstream corner occurs for the 15° wedge approximately over the range $37° < \delta < 45°$. For the first two shocks in Fig. 4a, δ more than spans this range, yet it can be seen that the shift has had virtually no effect on the body-shock geometry in the stagnation region. Note that the angles of attack for these first two shocks are such as to include all the present pressure data in Fig. 3. For our experiments the calculated wedge shock detachment angle is $\delta = 50°$, corresponding to $\alpha = 35°$. Thus, for the shocks with $35° < \alpha < 55°$, neither an asymptotic constant pressure nor an asymtotically straight shock exists any longer. In this range a noticeable thickening of the shock layer in the nose region is apparent, and it would seem, as far as the nose is concerned, that shock geometry has been influenced not by the sonic point shift but rather by the loss of asymptotic wedge flow.

This observation led to a closer examination of the interpretation of Johnson[5] of his cone-sphere experiments in helium at $M_\infty = 22$. A critical afterbody cone angle of 51° is reported in Ref. 5 below which shock detachment is independent of cone angle and above which shock detachment increases rapidly with cone angle. For $\gamma = \frac{5}{3}$, $M_\infty = \infty$, the cone shock detachment angle is 51.2°. This raises the suspicion that, in those experiments also, what is critical is loss of asymptotic flow rather than sonic point movement. We can obtain a direct comparison of this effect between blunted wedges and blunted cones. Shock standoff distance becomes difficult to define with asymmetry and a curved stagnation streamline, but we may note that, for the $\alpha = 15°$ shock, on the slender wedge well before sonic point shift and therefore typical for a cylinder, $\Delta/R = 0.36 \pm 0.01$. This may be compared to a cylinder value of $\Delta/R = 0.383$ obtained from Table 1 of Ref. 11 with $\gamma = 1.4$ and $M_\infty = 20$. We now use the $\alpha = 0$ shock for the 60° afterbody model, which yields $\Delta/R = 0.78 \pm 0.01$. This case is 10° past the calculated detachment angle, and the shock standoff distance is more than twice as large as that for the slender wedge. Shock standoff distance 10° past the crtical angle in Ref. 5 is larger than that for a sphere by a factor of nearly three.

The difference in shock shape with and without a strongly asymmetrical stagnation region is observable directly in Fig. 5. Here the 15° and 60° models with their shocks have been superimposed for the three indicated flow directions. It is seen that despite the fact that the flow deflection angle is the same on the upper sides of the two models, the shocks there are increasingly affected by the difference in the models on the opposite side as the angle of attack of the 15° model decreases. In Fig. 5a both upper sides but neither of the lower sides are past the detachment angle. In Fig. 5b both upper sides and the lower side of the 60° model are past this angle, and in Fig. 5c only the lower side of the 60° model has no asymptotic wedge flow. The fairly large influence of the lower side on the upper shown in Fig. 5c should be kept in mind in relation to the convenient and often used scheme whereby nonsymmetrical configurations are approximated by two supposedly equivalent symmetrical ones. At least for two-dimensional configurations, without cross-flow, this method can be very poor.

V. Modified Correlation from Hypersonic Slender Body Theory

Afterbody pressures and shock geometry for blunted wedges with various semiangles can be fruitfully examined through the correlations established by hypersonic slender body theory if these angles are small enough. It is required that both $M_\infty^2 \tan^2\theta \gg 1$ and $\tan^2\theta \ll 1$. Although the first condition is satisfied in the present experiments, the second is not. Nevertheless, we pursue the matter further.

Hypersonic slender body theory contains different types of solutions for various cases. For a blunted slender wedge or cone with small semiangle δ, a solution exists which results in a universal surface pressure distribution and shock shape for all values of δ, this angle having been incorporated into both pressure and position coordinates. The case of $\delta = 0$ is not included, however. For that case, i.e., that of a blunted flat plate or cylinder, the blast wave solution applies. This results in another set of variables which does not contain δ.

A unification of these two cases is contained in a transformation of the variables recently given by Greenberg.[13] This results in a single set of correlation parameters for the pressure on both a blunted cone and a blunted cylinder. One of these new variables is simply the pressure nondimensionalized with the asymptotic pressure. Figure 2 of Ref. 13 shows that p/p_{asy} correlates a variety of experimental and numerical data including cylindrical and conical afterbodies in terms of the new dimensionless body coordinate along the flow. No comparison to theory is made. Some of this data is for large values of δ up to 40°. The point to note here is that, through use of p_{asy}, the proper asymptotic limit is bound to be reached, not just for small δ as well as $\delta = 0$, but for any δ. The correlation is thus forced to be correct far downstream regardless of any slenderness restrictions.

In the following we extend this idea and give a correlation for both shock shapes and pressures for blunted cones or cylinders and wedges or flat plates. The present experimental large δ data (below loss of asymtotic flow) are then correlated on this basis and compared to slender body theory.

Pressure Correlation

First we consider the pressure for $\delta = 0$. For a given gas and very large M_∞, similarity considerations give the pressure

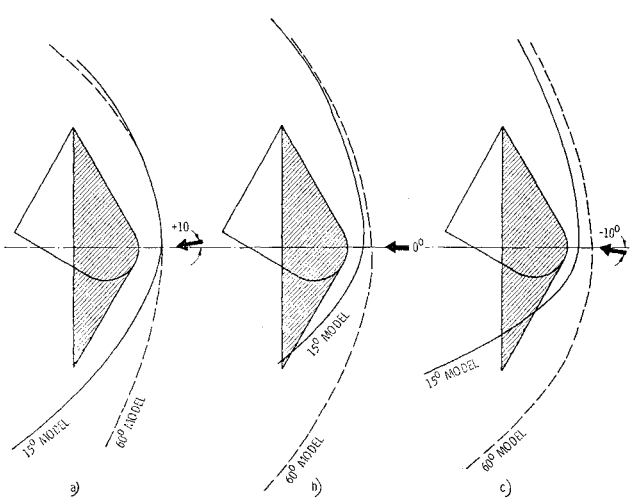

Fig. 5 Effect of asymmetric stagnation region.

in the functional form (pp. 208 and 213, Ref. 14)

$$p/p_\infty = f(x/d \cdot C_D{}^{-1/\nu} \cdot M_\infty{}^{-(2+\nu)/\nu})$$

Here C_D is the nose drag coefficient, ν is a geometrical factor which is unity for two-dimensional flow and two for axisymmetric flow, d is the nose thickness or diameter, and x is distance along the direction of flow measured from the nose. Since, for $\delta = 0$,

$$p_{asy} = p_\infty \qquad p_{max}/p_\infty = p_{max}/p_{asy} \sim M_\infty{}^2$$

we may write

$$\frac{p}{p_{asy}} = g\left[\frac{x}{d} \cdot C_D{}^{-1/\nu} \cdot \left(\frac{p_{asy}}{p_{max}}\right)^{(2+\nu)/2\nu}\right] \qquad (1)$$

Next, consider the pressure on a blunt-nosed slender wedge or cone, $\delta \neq 0$ but small. Now we have (p. 234, Ref. 14) a different functional relation that may be written

$$p/p_\infty = (M_\infty\delta)^2 f_\delta(x/d \cdot C_D{}^{-1/\nu} \cdot \delta^{(2+\nu)/\nu})$$

But within the limits of hypersonic slender body theory,

$$p_{asy}/p_\infty \sim (M_\infty\delta)^2 \qquad p_{asy}/p_{max} \sim \delta^2$$

We then obtain

$$\frac{p}{p_{asy}} = g_\delta\left[\frac{x}{d} \cdot C_D{}^{-1/\nu}\left(\frac{p_{asy}}{p_{max}}\right)^{(2+\nu)/2\nu}\right] \qquad (2)$$

For $\nu = 2$ this is the form obtained by Greenberg.[13] Although the functions involved in Eqs. (1) and (2) are different, the variables are the same. These variables will be the basis of our correlation. The functions are known theoretically for both $\nu = 1$ and $\nu = 2$. The function in Eq. (1) is given analytically by blast-wave theory, that in Eq. (2) can be obtained from different numerical solutions given by Chernyi[14] and Cheng.[15, 16] (Reference 16 contains results for blunted cones.) Since we wish to compare these solutions, especially those of Chernyi and Cheng, and since the numerical solution of Chernyi is given only for a perfect gas with $\gamma = 1.4$, this restriction is now imposed on the theories.

With $\gamma = 1.4$, the blast-wave equations for blunted plate and cylinder, Eqs. (5.4) and (5.6) of Ref. 14, may be transformed to the present coordinates to give

$$\frac{p}{p_{asy}} = 1 + \frac{0.146}{[(2x/C_Dd)(p_{asy}/p_{max})^{3/2}]^{2/3}} \qquad (\nu = 1) \quad (1a)$$

$$\frac{p}{p_{asy}} = 1 + \frac{0.0365}{(2/C_D)^{1/2}(x/d)(p_{asy}/p_{max})} \qquad (\nu = 2) \quad (1b)$$

It should be noted that these equations cease to be valid as p approaches p_{asy}.

The function in Eq. (2) as determined by Chernyi is obtained from Ref. 14 with Fig. 5.10 for $\nu = 1$ and Fig. 5.13

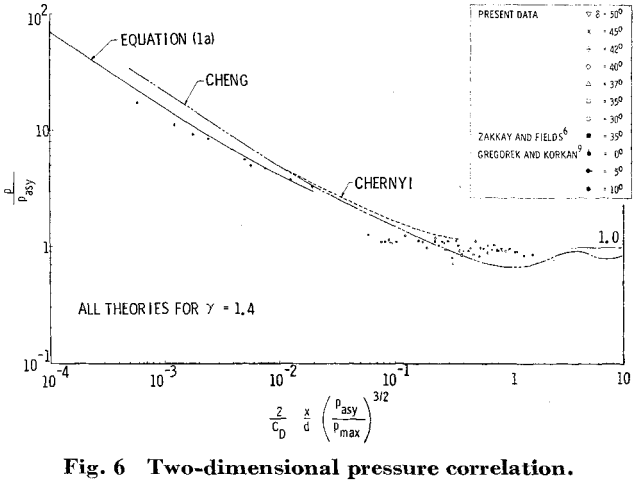

Fig. 6 Two-dimensional pressure correlation.

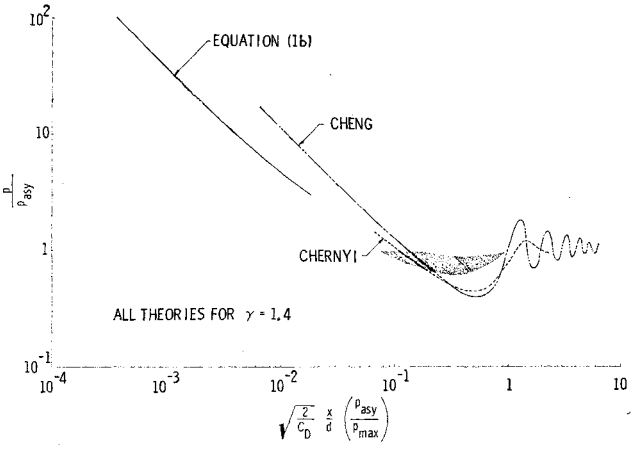

Fig. 7 Axisymmetric pressure correlation.

for $\nu = 2$ and the appropriate coordinate transformation. Correspondingly, this function, according to Cheng, can be obtained from Fig. 2.5 (b) of Ref. 15 for $\nu = 1$ and Fig. 6(B) of Ref. 16 for $\nu = 2$.

In Fig. 6 we show the two-dimensional results. Equation (1a) is indicated, as well as the results of Chernyi and Cheng, all for $\gamma = 1.4$. Cheng's pressure is considerably overexpanded with respect to the asymptotic-wedge pressure. His asymptotic pressure is below the wedge value; even if it were not, however, there would still be a region of overexpansion. Chernyi approaches the wedge value from above. The present real gas data begin with the first tap downstream of the cylinder-plate junction.§ They are seen to correlate quite well (the pressures from the corner taps have been eliminated), falling between the two theories and showing an overexpansion as previously indicated. The low Mach number data of Zakkay and Fields[6] now fit, as well as the experimental data of Gregorek and Korkan.[9] By drawing a straight line through the present data in Fig. 6, we obtain the previously described solid lines for the afterbody pressures in Fig. 3.

The axisymmetric case is shown in Fig. 7. Both the theories of Chernyi and Cheng show an overexpansion for this case, as is well known. Some data, including both experiments and method of characteristics calculations, have already been given in these coordinates by Greenberg[13]; the shaded region in Fig. 7 indicates where the overexpanded data in Ref. 13 fit with respect to the two theories.

Shock Correlation

Next, we consider shock shape away from the immediate vicinity of the nose, again first for $\delta = 0$. For this case we have (pp. 208 and 215, Ref. 14)

$$y/d \cdot C_D{}^{-1/\nu} \cdot M_\infty{}^{-2/\nu} = F(x/d \cdot C_D{}^{-1/\nu} \cdot M_\infty{}^{-(2+\nu)/\nu})$$

where y is the distance perpendicular to the flow direction from the stagnation streamline to the shock. By the previous argument for $\delta = 0$, this becomes

$$\frac{y}{d} \cdot C_D{}^{-1/\nu} \cdot \left(\frac{p_{asy}}{p_{max}}\right)^{1/\nu} = G\left[\frac{x}{d} \cdot C_D{}^{-1/\nu} \cdot \left(\frac{p_{asy}}{p_{max}}\right)^{(2+\nu)/2\nu}\right] \qquad (3)$$

For small but finite δ, the corresponding functional relation can be put in the form

$$y/d \cdot C_D{}^{-1/\nu} \cdot \delta^{2/\nu} = F_\delta(x/d \cdot C_D{}^{-1/\nu} \cdot \delta^{(2+\nu)/\nu})$$

By the previous small δ argument, this becomes

$$\frac{y}{d} \cdot C_D{}^{-1/\nu} \cdot \left(\frac{p_{asy}}{p_{max}}\right)^{1/\nu} = G_\delta\left[\frac{x}{d} \cdot C_D{}^{-1/\nu}\left(\frac{p_{asy}}{p_{max}}\right)^{(2+\nu)/2\nu}\right] \qquad (4)$$

§ The necessary C_D was taken as Newtonian over the nose that extends from the stagnation point to the wedge tangent point.

Again Eqs. (3) and (4) involve the same variables. This time, however, a further step is required to force the correlation to work asymptotically far downstream. Far downstream, for any finite δ, the shock must approach a straight shock given by $y = x\tan\theta$.

This can be put into the form

$$\frac{y}{d}\cdot C_D^{-1/\nu}\left(\frac{p_{asy}}{p_{max}}\right)^{1/\nu}\left[\left(\frac{p_{asy}}{p_{max}}\right)^{1/2}(\tan\theta)^{-1}\right] = \frac{x}{d}\cdot C_D^{-1/\nu}\left(\frac{p_{asy}}{p_{max}}\right)^{(2+\nu)/2\nu}$$

For small δ, the factor inside the bracket on the left is a constant, since small δ means small θ and $p_{asy}/p_{max} \sim \sin^2\theta \sim \tan^2\theta$. Then the functional form in Eq. (4) is indeed proper. For nonsmall δ, however, the bracket becomes proportional to $\cos\theta$, which we approximate as $(1 - p_{asy}/p_{max})^{1/2}$. For small δ this differs but little from unity. Thus, if we introduce this correction factor into the shock coordinate, we obtain as generalized shock correlation parameters

$$\frac{y}{d}\cdot C_D^{-1/\nu}\left(\frac{p_{asy}}{p_{max}}\right)^{1/\nu}\left(1-\frac{p_{asy}}{p_{max}}\right)^{1/2} = \mathfrak{F}\left[\frac{x}{d}\cdot C_D^{-1/\nu}\left(\frac{p_{asy}}{p_{max}}\right)^{(2+\nu)/2\nu}\right]$$

The following theoretical forms of the functional relationship are again restricted to $\gamma = 1.4$. For $\delta = 0$, we may write the blast wave results, Eqs. (5.5) and (5.7) of Ref. 14, as

$$\frac{2y}{C_D d}\frac{p_{asy}}{p_{max}}\left(1-\frac{p_{asy}}{p_{max}}\right)^{1/2} = 1.01\left[\frac{2x}{C_D d}\left(\frac{p_{asy}}{p_{max}}\right)^{3/2}\right]^{2/3} \qquad (\nu = 1) \quad (3a)$$

$$\left(\frac{2}{C_D}\right)^{1/2}\frac{y}{d}\left(\frac{p_{asy}}{p_{max}}\right)^{1/2}\left(1-\frac{p_{asy}}{p_{max}}\right)^{1/2} = 0.95\left[\left(\frac{2}{C_D}\right)^{1/2}\frac{x}{d}\frac{p_{asy}}{p_{max}}\right]^{1/2} \qquad (\nu = 2) \quad (3b)$$

Again by the previous restriction, these only hold up to a limiting value of the parameter on the right.

For small but finite δ, the shock for $\nu = 1$ according to Chernyi comes from Fig. 5.9 of Ref. 14 (no y is given there for $\nu = 2$). The shock according to Cheng can be obtained for $\nu = 1$ from Fig. 2.5(a) of Ref. 15 and for $\nu = 2$ from Fig. 6(a) of Ref. 16.

These theoretical results, as well as some shocks from the present experiments, appear in Fig. 8. Agreement between the blast wave solutions and the small but finite δ solutions for shock shape is considerably better than for the pressures. Further, in these coordinates the transition far downstream to a straight shock occurs conveniently at about the same place for both the axisymmetric and two-dimensional cases. Four experimental shocks are given for $\delta = 30°$, 45°, and 50° taken from the windside on the 15° model and for $\delta = 0$ taken from the shadowside at $\alpha = 15°$. The points begin in the immediate vicinity of the nose-afterbody junction. There are two sets for $\delta = 30°$ and $\delta = 50°$, obtained from different frames of the film for the appropriate run, to give an idea of the over-all accuracy in shock position. The collapse of the data is quite good. Both the $\delta = 0$ and the large δ data appear to be approaching the relevant theoretical curves ($\nu = 1$), although the initial points are relatively far away. This departure is, however, to be expected in view of their nearness to the nose.

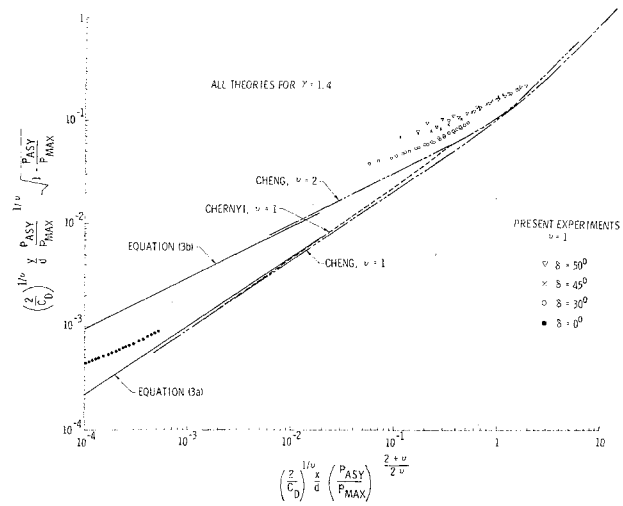

Fig. 8 Shock correlations.

VI. Concluding Remarks

The results of the present experiment on blunted wedges indicate that relatively little significance is to be attached to a sonic point shift from the nose to the downstream corner.

Loss of asymptotic wedge flow, on the other hand, can have important consequences in changing shock standoff distance for symmetrical bodies and in coupling wind and shadow sides when symmetry does not exist.

In this connection it is of interest to recall the very early scheme of Moeckel[1] for predicting the detached shock on a blunt body, with or without symmetry. The method approximates the sonic point location on any body by the point of tangency of the body and a line parallel to the cone or wedge corresponding to shock detachment, or by a corner if the body ahead of the corner is everywhere steeper than this angle. Further, the sonic line is taken to be straight and normal to the average flow direction across it. The shock standoff distance is then related to the body thickness at the approximated sonic point. For conditions such as studied in the present experiments, neither approximation is valid, since the actual sonic point has been made to shift much further downstream than this approximate one. The sonic line is then not straight, being essentially normal to the flow near the shock but parallel to it near the body. But if the nose-induced entropy layer near the surface is sufficiently thin, this downstream stretching of the sonic line will affect only a small part of the flow field and, therefore, not matter. The new actual location of the sonic point will only begin to matter when the sonic point on the shock has also shifted, i.e., when the afterbody angle becomes the detachment angle. Then the approximated sonic point again agrees with the actual sonic point. Thus, the transonic characteristics implied in the Moeckel method are essentially correct and should provide a useful guide even under conditions leading to a large shift in the sonic point, provided the approximately located special point is not taken literally as the sonic point.

It has been shown that there exists a transformation that results in the same set of variables for both the case of a blunted wedge or cone with small but finite afterbody deflection angle δ and that with zero flow deflection angle. This can then be modified so as to be asymptotically correct even with large angles for both shock shape and surface pressure. In the new coordinates the present measured surface pressures and shocks for large δ correlate quite well with small δ theory. This is true even for angles of attack so large that the surface is subsonic. This conclusion is qualified by the important restriction that with a subsonic corner the corner must not be too close to the nose, since otherwise the subsonic afterbody pressure is determined by the corner. For large δ, blunting can induce pressures below the asymptotic pressure for two-dimensional as well as axisymmetric flow.

Finally, it is hoped that the results of the experiment as expressed in the present coordinates may stimulate theoretical work toward a unification of not only the coordinates but the functions involved as well.

References

[1] Moeckel, W. E., "Approximate method for predicting form and location of detached shock waves ahead of plane or axially symmetric bodies," NACA TN 1921 (July 1949).

[2] Maslen, S. H., "Inviscid hypersonic flow past smooth bodies," AIAA J. **2**, 1055–1061 (1964).

[3] Holt, M., "Direct calculation of pressure distribution on blunt hypersonic nose shapes with sharp corners," J. Aerospace Sci. **28**, 872–876 (1961).

[4] Vaglio-Laurin, R., "On the PLK method and the supersonic blunt body problem," J. Aerospace Sci. **29**, 185–206 (1962).

[5] Johnson, R. H., "The cone-sphere in hypersonic helium above Mach number twenty," Aerospace Eng. **18**, 30–34 (February 1959).

[6] Zakkay, V. and Fields, A. K., "Pressure distributions on a two-dimensional blunt-nosed body at various angles of attack," Polytechnic Institute of Brooklyn, PIBAL Rept. 461 (October 1958).

[7] Humphrey, R. L., Little, W. J., and Seeley, L. A., "Mollier diagram for nitrogen," Arnold Engineering Development Center, AEDC TN-60-83 (May 1960).

[8] Ahtye, W. F. and Peng, T. C., "Approximations for the thermodynamic and transport properties of high temperature nitrogen with shock tube applications," NASA TN D-1303 (July 1962).

[9] Gregorek, G. M. and Korkan, K. D., "An experimental observation of the Mach- and Reynolds-number independence of cylinders in hypersonic flow," AIAA J. **1**, 210–211 (1963).

[10] Hamaker, F. M., "Numerical solution of the flow of a perfect gas over a circular cylinder at infinite Mach number," NASA Memo. 2-25-59A (March 1959).

[11] Fuller, F. B., "Numerical solutions for supersonic flow of an ideal gas around blunt two-dimensional bodies," NASA TN D-791 (July 1961).

[12] Penland, J. A., "Aerodynamic characteristics of a circular cylinder at Mach number 6.86 and angles of attack up to 90°," NACA TN 3861 (1957).

[13] Greenberg, R. A., "A correlation of nose-bluntness-induced pressures on cylindrical and conical afterbodies at hypersonic speeds," J. Aerospace Sci. **29**, 359 (1962).

[14] Chernyi, G. G., *Introduction to Hypersonic Flow* (Academic Press, New York, 1961).

[15] Cheng, H. K., Hall, J. G., Golian, T. C., and Hertzberg, A., "Boundary-layer displacement and leading-edge bluntness effects in high-temperature hypersonic flow," J. Aerospace Sci. **28**, 353–381 (1961).

[16] Cheng, H. K., "Hypersonic flow with combined leading-edge bluntness and boundary-layer displacement effect," Cornell Aeronautical Lab. Rept. AF-1285-A-4 (August 1960).

SEPTEMBER 1964 AIAA JOURNAL VOL. 2, NO. 9

Recent Studies of the Laminar Base-Flow Region

ERIC BAUM,* HARTLEY H. KING,† AND M. RICHARD DENISON‡

Electro-Optical Systems, Inc., Pasadena, Calif.

Some recent theoretical studies of the fluid dynamics and energy transport in the laminar base-flow region are presented. Improvements to Chapman's separated flow analysis include the effect of finite initial profiles at the separation point, the effects of mass injection from the body surface or base, and the influence of base heat transfer. Some of the more important conclusions are that 1) the Crocco integral relation for the enthalpy and atom distributions in the separated shear layer is not valid for most hypersonic bodies because the base-flow region is far too short for the profiles to have become similar; 2) the distortion of initial profiles due to a sharp turn at the separation point results in a shorter and cooler base flow, as compared to using undistorted initial profiles; 3) base heat transfer appears to have only a slight effect on base-flow properties; and 4) both base gas injection and similar blowing from the body wall result in a cooler and longer base-flow region, base injection being the more effective in cooling the wake for equal mass injection rates.

Nomenclature

B = blowing parameter
DSL = dividing streamline
E = auxiliary enthalpy function, Eq. (12)
ESL = inviscid flow streamline outside viscous layer, Fig. 3
F = shear function, Eq. (6)
f = Blasius function
H = total enthalpy, $h + u^2/2$
k = 0 for two-dimensional flow, 1 for axisymmetric flow
M = Mach number
$\dot{M}$ = injection mass flow rate (per unit depth, two-dimensional, total, three-dimensional)
Re = Reynolds number
r_0 = radius of viscous layer
S = reduced streamwise distance, Eq. (4)
SSL = stagnating streamline
u = streamwise velocity
v = transverse velocity
W = auxiliary enthalpy function, Eq. (12)
x = streamwise distance
Y = transformed normal distance, Eq. (7)
y = transverse distance
z = distance along centerline from base
α = cone half angle
β = wake angle
μ = viscosity
ρ = density
τ = shear stress
ψ = stream function

Subscripts

b = base wall
c = recirculating core

Presented as Preprint 64-5 at the AIAA Aerospace Sciences Meeting, Pasadena, Calif., January 20–22, 1964. This research was sponsored by the Advanced Research Projects Agency, Department of Defense under ARPA Order 203-A1-63. The authors are indebted to Lester Lees of the California Institute of Technology, Martin H. Bloom of the Polytechnic Institute of Brooklyn, and Andrew Hammitt and Leslie Hromas of Space Technology Laboratories for many valuable discussions.

* Senior Scientist. Member AIAA.

† Senior Engineer. Member AIAA.

‡ Manager, Gas Dynamics Department. Member AIAA.